Pure Appl. Chem., Vol. 72, Nos. 1–2, pp. 21–33, 2000.

Metal nanoparticles, nanowires, and carbon nanotubes*

C. N. R. Rao[1,2,3†], G. U. Kulkarni[1], A. Govindaraj[3], B. C. Satishkumar[1], and P. John Thomas[1]

[1]Chemistry and Physics of Materials Unit or [2]CSIR Centre of Excellence in Chemistry, Jawaharlal Nehru Centre for Advanced Scientific Research, Jakkur P.O. Bangalore 560 064, India; [3]Solid State and Structural Chemistry Unit, Indian Institute of Science, Bangalore 560 012, India

Abstract: The size-dependent metal to nonmetal transition in metal nanoparticles has been investigated using photoelectron and tunneling spectroscopic techniques. Metal nanoparticles capped by thiols are shown to organize into ordered 2D and 3D structures. Single-walled nanotubes and aligned carbon nanotube bundles have been synthesized by controlling the size of metal nanoparticles produced *in situ* during the pyrolysis of precursors. Nanowires of gold and other metals have been produced in the capillaries of the single-walled nanotubes.

INTRODUCTION

Electron transport in nanostructures, in particular in quantum dots and their arrays, is not only of academic interest, but also holds promise in nanoelectronics [1–3]. Synthesis of metal nanoparticles and nanowires of desired properties, therefore, assumes significance. Carbon nanotubes constitute yet another related class of materials with several potential applications in electronics [4]. Of particular relevance in this context, is the synthesis of aligned nanotube bundles.

In the last few years, metal nanoparticles have been investigated by various chemical and physical methods [1]. Size-dependent electronic structure of the nanoparticles is the focus of these studies. It is generally known that the conduction band present in a bulk metal will be absent in a nanoparticle, and instead there would be discrete states at the band edge. Electrons may therefore undergo quantum-confinement in very small metal particle, showing properties of a quantum dot [2]. Of particular interest are assemblies of colloidal particles [5], wherein metal nanoparticles, suitably covered by organic molecules such as thiols, get self-organized in crystalline arrays of one, two, or three dimensions. Electron transport in such mesostructures is equally interesting. In this article, we briefly present the size-dependent electronic properties of the metal particles we investigated and provide some highlights of their assemblies in two and three dimensions. We also present the synthesis of bundles of aligned carbon nanotubes employing a pyrolysis method where magnetic metal nanoparticles produced *in situ* play a crucial role. Metal nanowires produced in the capillaries of single-walled nanotubes are also discussed.

ELECTRONIC STRUCTURE OF METAL NANOPARTICLES

The electronic structure of a metal particle critically depends on its size. For small particles, the electronic states are not continuous, but discrete, due to confinement of the electron wavefunction. The average spacing of successive quantum levels, δ, known as the Kubo gap, is given by $\delta = 4E_f/3n$, where E_f is the

Pure Appl. Chem.* **72, 1–331 (2000). An issue of reviews and research papers based on lectures presented at the 1st IUPAC Workshop on Advanced Materials (WAM1), Hong Kong, July 1999, on the theme of nanostructured systems.
†Corresponding author: E-mail: cnrrao@jncasr.ac.in

Fermi energy of the bulk metal and *n* is the number of valence electrons in the nanoparticle (usually taken as its nuclearity). Thus, for a Ag nanoparticle of 3-nm diameter containing ~10^3 atoms, the value of δ would be 5–10 meV. Since at room temperature, $kT \cong 25$ meV, the 3-nm particle would be metallic ($kT > \delta$). At low temperatures, the level spacings especially in small particles, may become comparable to *k*T, rendering them nonmetallic [2]. Because of the presence of the Kubo gap, properties such as electrical conductivity and magnetic susceptibility exhibit quantum size effects. Discreteness of energy levels also brings about changes in the spectral features, especially those related to the valence band.

High-energy spectroscopies provide a direct access to the electronic structure of metal nanoparticles. In X-ray photoelectron spectroscopy (XPS), the kinetic energy of the photoelectron ejected from an atomic core-level is measured to determine the binding energy of that level. Ultraviolet photoelectron spectroscopy (UPS) and bremmstrahlung isochromat spectroscopy (BIS), on the other hand, provide information on the occupied and unoccupied levels respectively near E_f. In the last few years, several experiments have been carried out on nanoparticles in the desired size range obtained by the deposition of metals on amorphized graphite and other substrates, using electron spectroscopic techniques [6,7]. The particles were obtained by the resistive evaporation of the corresponding metal in vacuum. The variation in the core-level binding energy of the nanoparticle with respect to the bulk metal value has been measured as a function of the coverage or particle size for metals such as Au, Ag, Pd, Ni, and Cu. An important result from these experiments is that as the particle size decreases, the binding energy increases sharply by as much as 1.2 eV as in the case of Pd (Fig. 1). The variation is negligible at large coverages or particle size since the binding energies would be close to those of the bulk metals. The increase in the core-level binding energy in small particles occurs due to the poor screening of the core-hole and is a manifestation of the size-induced metal–insulator transition in nanoparticles.

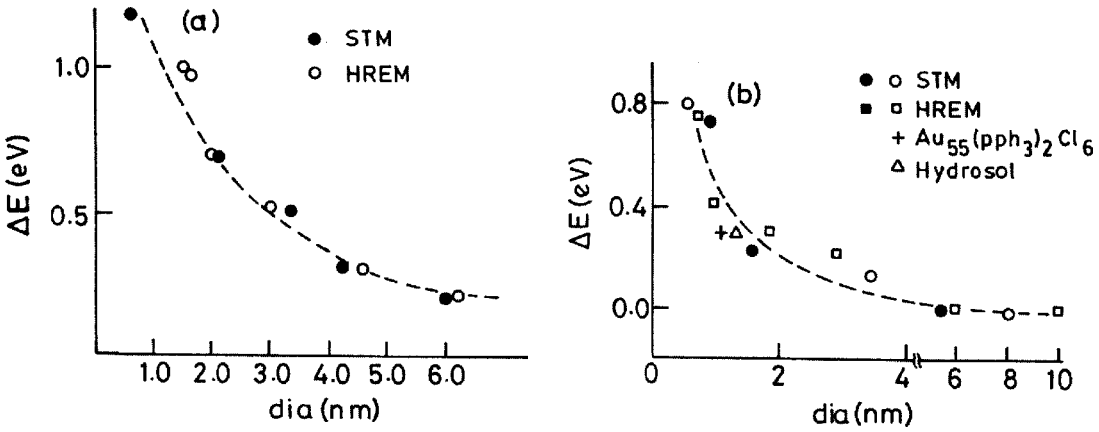

Fig. 1 Variation of the shifts in the core-level binding energies (relative to the bulk metal value) of Pd (a) and Au (b) clusters, with the average diameter of the cluster. The diameters were obtained from HREM and STM images. In the case of Au clusters, data for a colloidal particle and a Au_{55} compound are also shown.

The electronic band structure of metal nanoparticles near the Fermi level as revealed by UPS and BIS techniques is of considerable interest [6–8]. In Fig. 2 we show typical spectra of Pd nanoparticles. For large particles (~5 nm diameter), the UP spectrum is similar to that of the bulk metal, where a considerable intensity is present at E_f due to the Pd(4d) states arising from the metallic nature of the nanoparticles. For small particles (<2 nm diameter), however, the intensity of the 4d states at E_f decreases rapidly, accompanied by a shift in the intensity maximum to higher binding energies and a narrowing of the 4d-related spectral features. The BI spectra of small nanoparticles show that the empty

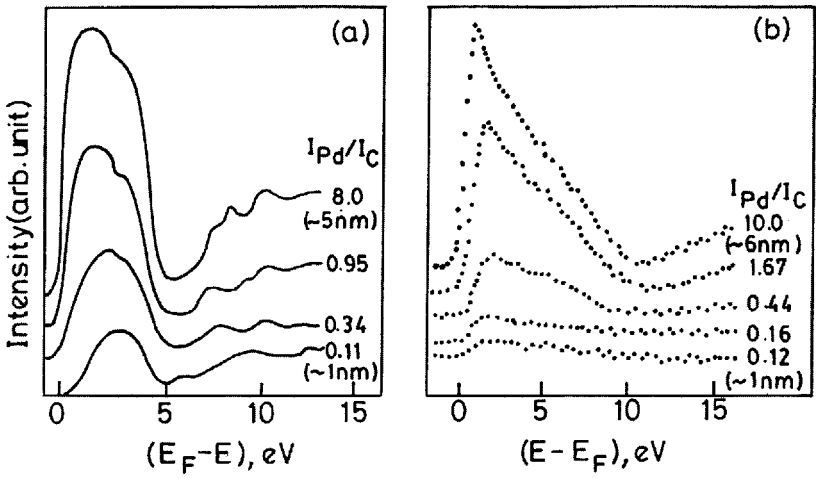

Fig. 2 Electronic structure of small Pd clusters near the Fermi level. (a) He II UP spectra show a decrease in the intensity of the occupied 4d band with the decreasing cluster size. This is accompanied by a shift in the intensity maximum to higher binding energies and a narrowing of the spectral features. (b) BI spectra show similar effects in the empty 4d states above the Fermi level. I_{Pd}/I_C values (ratios of XPS core-level intensities of Pd and the graphite substrates) are used as a measure of the coverage or the cluster size. The approximate cluster diameter is indicated in extreme cases.

4d states have negligible intensity at E_f. With the increasing particle size, new states emerge closer to E_f resembling the spectrum of bulk metal. Thus, both UP and BI spectra establish the emergence of new states at E_f with the increase in the particle size, consistent with the occurrence of an insulator-to-metal transition. Similarly, the BI spectra of Ag nanoparticles show a distinct feature that moves towards the E_f with increase in size, accompanied by an increase in the intensity of the 5s band. All these electron spectroscopic measurements indicate that a gap manifests itself around a nanoparticle diameter of 1–2 nm possessing 300 ± 100 atoms. Recent photoelectron spectroscopic measurements [8] on mass-selected Hg_n nanoparticles (n = 3 to 250) reveal that the HOMO-LUMO (*s*-*p*) gap decreases gradually from ~3.5 eV for n = 3 to ~ 0.2 eV for n = 250. The bandgap closure is predicted at n ~ 400. In metal colloids, surface plasmon excitations impart characteristic colors to the metal sols, the wine-red color of the gold sols being well-known. We found that colloidal particles of 4.2 and 2.1 nm diameters exhibit a distinct band around ~525 nm [9], the intensity of which increases with size. The intensity of this feature becomes rather small in the case of the 1-nm-diameter particles (≤200 atoms).

Direct information on the nonmetallic gap states in nanoparticles is obtained by scanning tunneling spectroscopy (STS). This technique provides the desired sensitivity and spatial resolution, making it possible to carry out tunneling spectroscopic measurements on individual particles. A systematic STS study of Pd, Ag, Cd, and Au nanoparticles of varying sizes deposited on a HOPG substrate has been carried out recently under ultra-high vacuum conditions, after having characterized the nanoparticles by XPS and STM [10]. The overall slope of the I-V curve near zero-bias, which is related to the density of states (DOS) near E_f, increases linearly up to particle volume of ~4 nm^3 (~2 nm diameter) and becomes constant for bigger particles as shown in Fig. 3a. Accordingly, the DOS in particles with a diameter >2 nm (with ~300 atoms or more) resembles that of the bulk. Derivative spectra of bigger particles were featureless, while those of the small particles (<1 nm) showed well-defined peaks on either side of zero-bias due to the presence of a gap. Ignoring gap values below 25 meV (~kT), it is seen that small particles of ≤1 nm diameter are nonmetallic (Fig. 3b). This observation is consistent with the

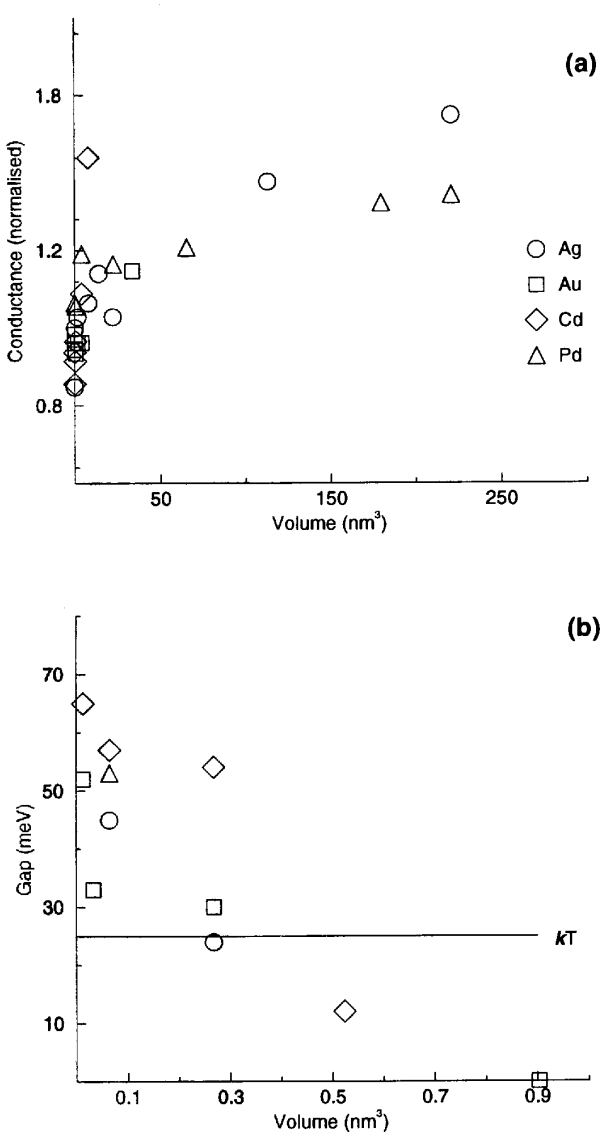

Fig. 3 Scanning tunneling spectroscopy of individual metal clusters: (a) Conductance (obtained from the normalized slope of the I-V curves) as a function of cluster volume. Above a critical volume ~4 nm^3, the slope becomes size-independent. (b) The conduction gap observed in small clusters of Au, Pd, Cd, and Ag as a function of cluster volume. The volume was calculated from the cluster diameter obtained from STM.

absence of the plasmon band in nanoparticles of 1 nm diameter. From the various studies discussed hitherto, it appears that the size-induced metal-insulator transition in metal nanoparticles occurs in the range of 1–2 nm dia or 300 ± 100 atoms. Theoretical investigations of the electronic structure of metal nanoparticles also throw light on the size-induced changes in the electronic structure. Rosenblit and Jortner [11] calculated the electronic structure of a model metal cluster and predicted electron localization to occur in a cluster of diameter ~0.6 nm.

Bimetallic nanoparticles

Bimetallic or alloy colloids have been made by the chemical reduction of the appropriate salt mixtures in solution phase. Thus, Ag–Pd and Cu–Pd colloids of varying compositions have been prepared by alcohol reduction of $AgNO_3$+PdO_x and CuO_x+PdO_x mixtures [12]. Ag–Pt colloids have been prepared by the $NaBH_4$ reduction of oxalate precursors and Cu–Pd colloids by the thermal decomposition of

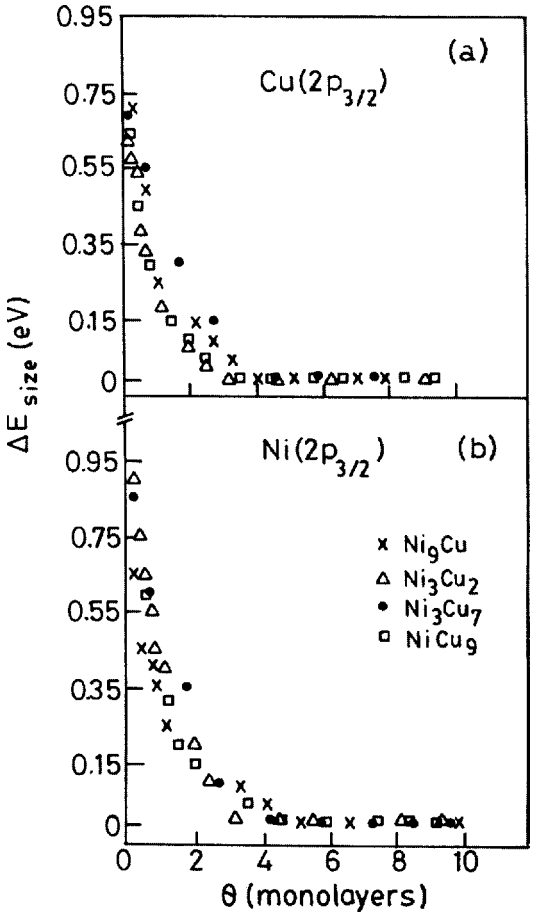

Fig. 4 Coverage or cluster size dependence of the shift in the $2p_{3/2}$ binding energy of (a) Cu and (b) Ni in Cu–Ni bimetallic clusters.

acetate mixtures in high-boiling solvents. Several bare bimetallic nanoparticles have been deposited on solid substrates by thermal evaporation in vacuum [13]. Examples of such alloy nanoparticles are Ni–Cu, Ag–Au, Ni–Pd and Cu–Pd. Measurements of the core-level binding energies of the component metals in the alloy particles show that the shifts in binding energy (relative to those of bulk metals), ΔE, comprise additive contributions from alloying and the particle size. That is, the observed ΔE is given by, $\Delta E = \Delta E_{alloy} + \Delta E_{size}$. At large particle size, only the alloying effect, ΔE_{alloy}, is found as in bulk alloys. Small alloy particles exhibit the size effect, in that the ΔE_{size} shows a marked increase, with decrease in particle size. The effect due to particle size is shown in Fig. 4 in the case of Ni–Cu alloy nanoparticles.

NANOPARTICLE ASSEMBLIES

The quest for nanoscale architecture has demanded newer synthetic methodologies for forming and organizing metal particles. In this context, the use of self-assembling surfactants is of significance. Thus, metal nanoparticles capped with thiols, silanes, phospholipids, and phosphines can be prepared in solid form. We shall examine the recent results obtained with 2D and 3D assemblies of metal nanoparticles.

Two-dimensional arrays

Schiffrin and co-workers [14] first prepared gold organosols using alkane thiols as surfactants, by phase-transferring gold ions and carrying out reduction in the presence of the thiols. A novel method of thiol-

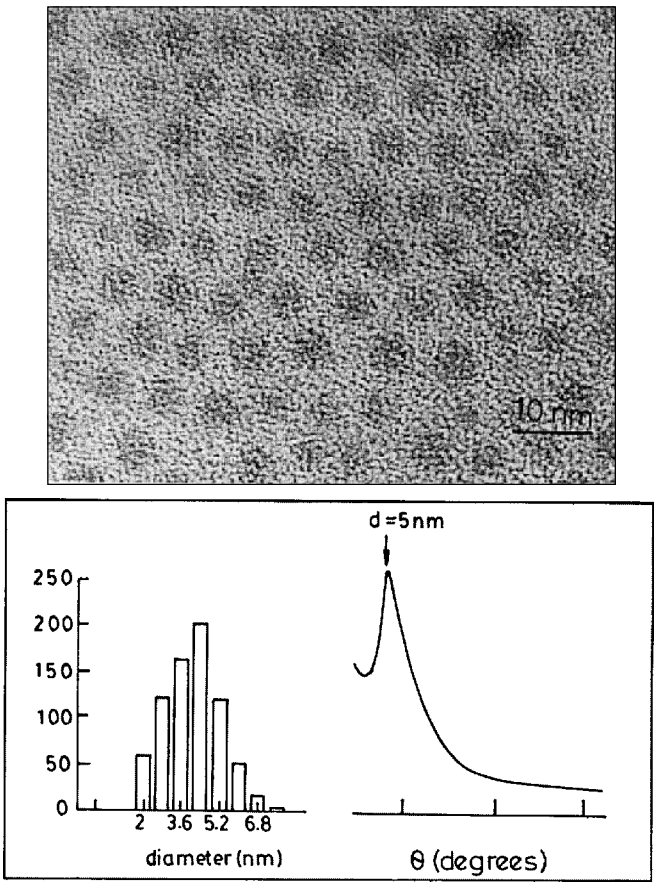

Fig. 5 2D array of thiol-derivatized Au particles of 4.2 nm mean diameter. Histograms indicating particle size distribution is given. XRD pattern from this array is also shown.

derivatizing hydrosols of various metals has been developed recently [15]. The procedure involves mixing a hydrosol containing metal particles of the desired size distribution with a toluene solution of an alkane thiol (butanethiol or higher members). The immiscible liquid layers thus obtained is stirred vigorously with HCl or $NaBH_4$ when the metal particles in the bottom aqueous layer gush to the upper hydrocarbon layer containing the thiol and get thiol-derivatized in this process. The completion of the derivatization is marked by a vivid interchange of the colors from the aqueous layer to the hydrocarbon layer. The advantage of this method is that well-characterized metal particles can be easily thiol-derivatized in a nonaqueous medium. Gold, silver, and platinum particles of different sizes have been thiolized by this procedure.

Thiolized metal nanoparticles from a nonaqueous medium are readily assembled into 2D arrays on a suitable solid substrate such as HOPG. As an example, the TEM image of a nanocrystalline array of gold particles with a mean diameter of 4.2 nm is shown in Fig. 5. The metal particles form close-packed structures extending over tens of nms with a regular spacing of ~1 nm between them [9]. X-ray diffraction pattern of this array exhibits a low-angle peak corresponding to a *d* spacing of 5.0 nm (Fig. 5). The distance between the particles deduced from the d-spacings is somewhat smaller than that expected from the dimensions of the metal particles and the thiol, suggesting some overlap of the alkane

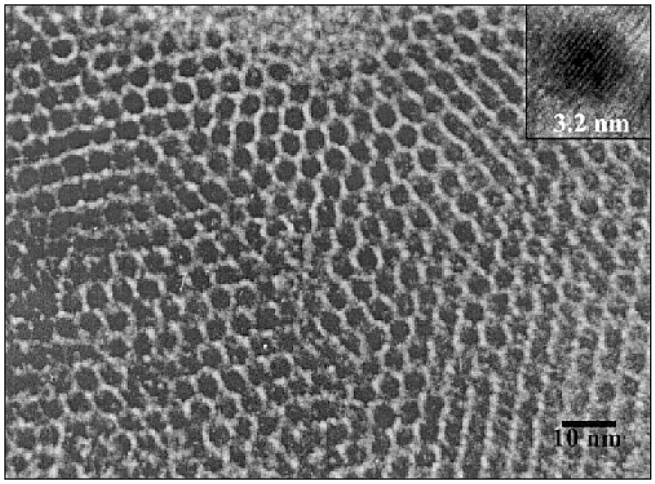

Fig. 6 TEM image of 2D array of thiol-derivatized Pd clusters of uniform size and nuclearity. Inset shows lattice fringes of individual clusters corresponding to a nuclearity of around 1400.

chains of the thiols on the neighboring particles. Ordered 2D lattices containing thiolized Au particles of two different sizes have been reported recently by Kiely et al. [16]. A careful study in this laboratory of 2D lattices formed by Pd nanoparticles of different sizes by employing alkane thiols of different lengths (butane to hexadecanethiol) has revealed some interesting aspects of particle assemblies. Ordered 2D lattices are formed with Pd particles in the diameter range of 2 to 6 nm with octanethiol and dodecanethiol. Satisfactory 2D lattices are generally observed when the ratio of the particle diameter (d) and the thiol chain length (l) is between 1 and 4, the most ordered lattices being favored when the d/l ratio is between 2 and 3.

It is of considerable value if one can prepare 2D lattices of metal quantum dots containing fixed number of atoms. Langmuir–Blodgett films containing Au_{55} nanoparticles have been obtained [17]. More interestingly, starting with cluster compounds of fixed nuclearity, it is possible to prepare the 2D lattices of thiolized Pd particles of uniform size. In Fig. 6, we show a TEM image of the 2D array of Pd particles, each containing around 1400 atoms.

Thiol-capped metal nanoparticles provide an excellent means of studying monoelectron conduction in metal quantum dots, giving rise to the Coulomb staircase phenomenon. In Fig. 7, we show how the charging energy of Au particles varies with the size. The Coulomb gap increases with the decrease in particle size as expected. The electronic structure of 2D lattices of metal quantum dots is of interest. A 2D lattice consisting of metal nanoparticles separated by a distance using an organic spacer serves as a model system to study the Mott–Hubbard metal–insulator transition wherein a decrease in the distance between the quantum dots (or increase in pressure) closes the Coulomb gap. By varying the interparticle distance continually in a 2D lattice of Ag particles (3 nm diameter) in a Langmuir trough, Collier et al. [18] have indeed found the Coulomb gap to vanish at a critical distance. We are examining metal particles linked by conjugated thiols and dithiols of varying lengths, in comparison with those of saturated thiols.

Three-dimensional superlattices

Multilayer assemblies using monothiols are generally fragile. Multilayer deposition of particle arrays is best achieved by the sequential adsorption of dithiol molecules and metal nanoparticles of the desired size, by dipping the substrate into the respective solutions with intermediate steps involving washing with toluene and drying [19]. Using this procedure, several monometal, bimetal, and metal-semiconductor superlattices have been prepared. The procedure is shown schematically in Fig. 8. As many as five

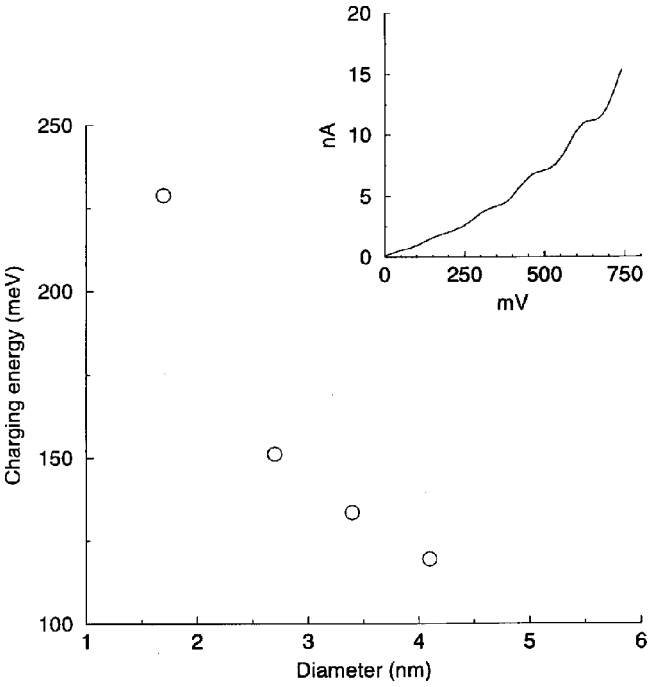

Fig. 7 Charging energies of PVP-covered gold nanoparticle of varying sizes. A coulomb staircase obtained with a 4-nm-diameter particle is shown in the inset.

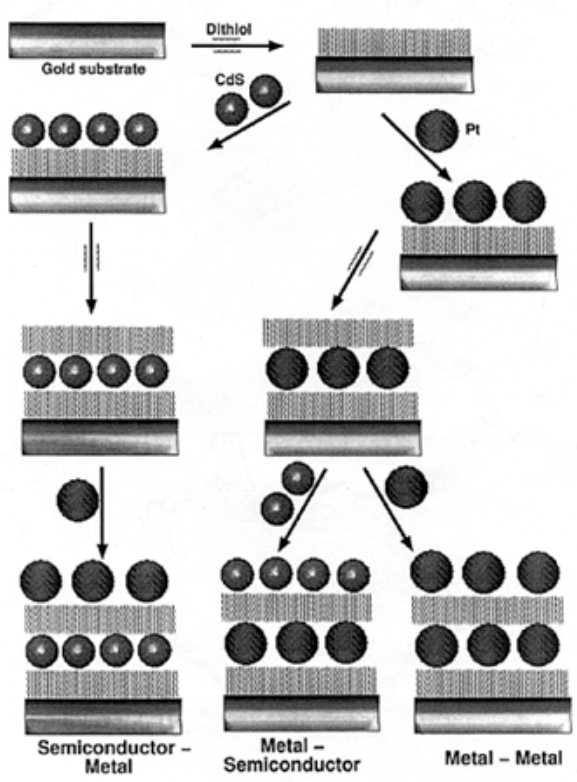

Fig. 8 Schematic drawing depicting the layer-by-layer deposition of Pt particles onto a Au substrate, the layers being separated by dithiol molecules. Also shown is the formation of a heterostructure consisting of alternate layers of semiconductor and metal particles.

depositions of nanocrystalline arrays could be accomplished by this method. After each deposition, the structure was characterized by STM and X-ray diffraction, as well as by XPS. STM images showed the presence of regular arrays of nanoparticles extending over 300 nm, corresponding to the size of a typical flat terrace on the substrate. The images also revealed a nearly regular spacing of 2 nm between the nanoparticles. XRD patterns recorded after successive depositions of layers exhibited low-angle reflections with the *d*-spacings reflecting the particle diameter and the inter-particle distance. The intensities of Pt(4f), C(1s) and S(2p) core-levels increased while Au(4f), due to the substrate, decreased with successive depositions. A plot of the metal coverage versus the number of depositions gave a slope close to unity until the third deposition and increased thereafter, suggesting that layer-by-layer deposition of nanoparticles had been accomplished.

ROLE OF METAL NANOPARTICLES IN THE FORMATION OF CARBON NANOTUBES

Depending on the size of the metal nanoparticles, pyrolysis of hydrocarbons produces single-walled nanotubes (SWNT), multiwalled nanotubes (MWNT), or metal-filled onions or graphene-covered metallic particles. We illustrate this in Fig. 9. Organized metal nanoparticles are used to produce aligned bundles of nanotubes by the pyrolysis of hydrocarbons. Small particles with diameters in the 1–2 nm range catalyze the formation of SWNTs while bigger particles of ~10–50 nm give rise to MWNTs. By controlling the partial pressure of the organometallic and hydrocarbon precursors, one can preferentially obtain SWNTs [20].

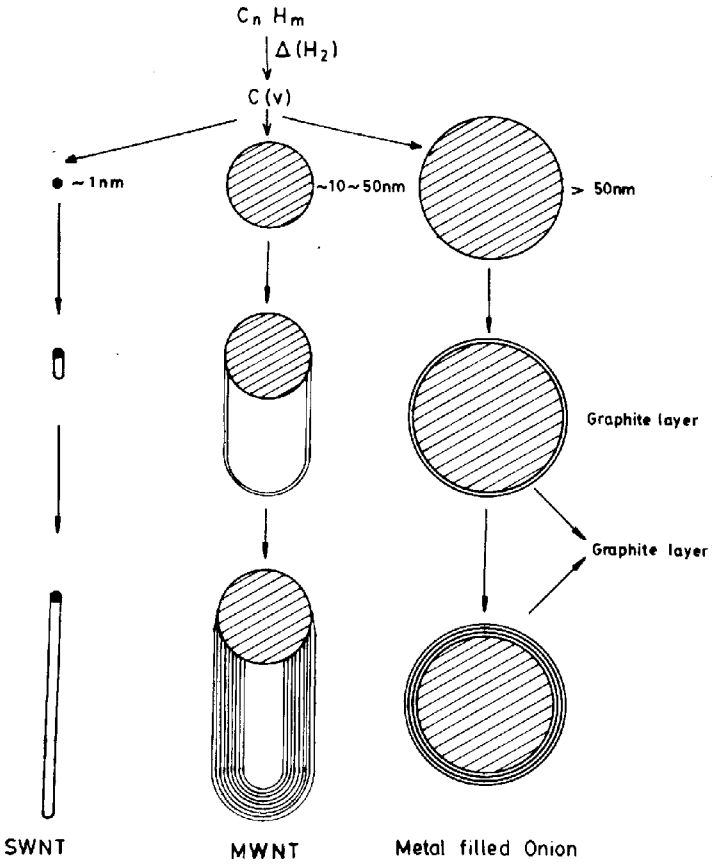

Fig. 9 Schematic illustration of the role of metal particles in the formation of carbon nanotubes by the pyrolysis method. Small particles (~1 nm) give rise to SWNT, bigger particles (~10 nm) produce MWNT while much larger particles (>50 nm) get encapsulated in graphite layers.

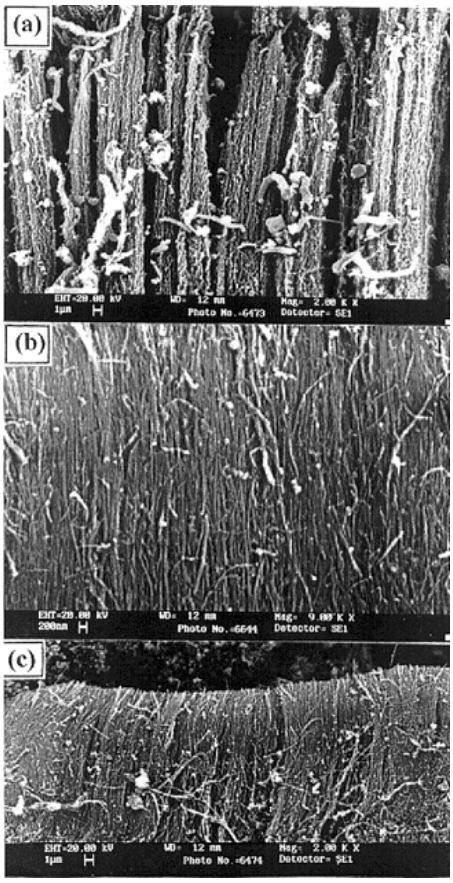

Fig. 10 SEM images (viewed perpendicular to the nanotube axis) of aligned nanotubes obtained from ferrocene–hydrocarbon mixtures; (a) methane, (b) acetylene, and (c) butane.

Aligned nanotube bundles have been obtained previously by chemical vapor deposition on laser-patterned substrates [21] or in porous solids [22,23]. We have produced aligned nanotubes by the pyrolysis of mixtures of organometallic precursors and hydrocarbons [24]. The advantage of this method is that aligned tubes may be produced in one step, without the use of a substrate. In Fig. 10, we show the SEM images of aligned nanotubes obtained by the pyrolysis of ferrocene with methane, acetylene, and butane respectively at 1373 K. The average length of the nanotubes was generally around 60 μm with methane and acetylene. Although the nanotubes are aligned in the case of methane (Fig. 10a), the packing density is not high. With acetylene, however, more compact nanotube bundles are obtained, as seen from Fig. 10b. A negligible proportion of graphene-covered metal nanoparticles were present along with the nanotubes when methane or acetylene were used as the hydrocarbon sources. When butane was used (Fig. 10c), there was a greater proportion of extraneous carbon deposits mainly consisting of Fe particles encapsulated inside graphitic sheaths. The average length of the nanotubes was also shorter.

In order to study the nature of the metal nanoparticles involved in the formation of the nanotube bundles, we have analyzed the samples using TEM. As an example, a TEM image of the nanotubes obtained by the pyrolysis of ferrocene–acetylene mixture is shown in Fig. 11. Iron nanoparticles sticking to the end portions of the nanotubes can be clearly seen. The particle diameters are in the range of 2–13 nm. Magnetization measurements carried out on this sample showed the saturation magnetization to be ~20 emu/g, which is considerably smaller than the bulk value of 222 emu/g. It is noteworthy that

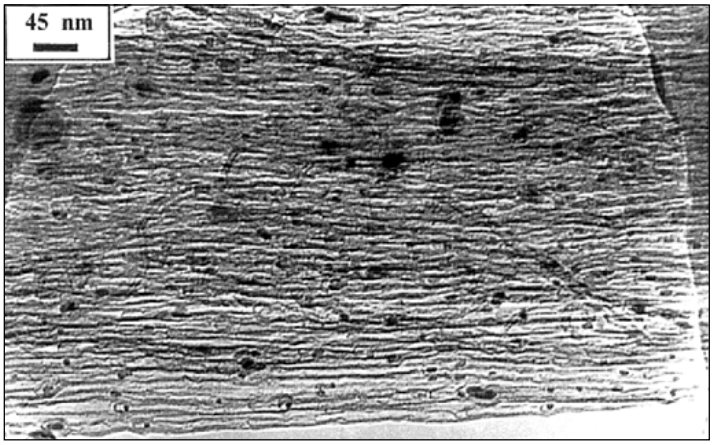

Fig. 11 TEM image of a part of an aligned nanotube bundle obtained from the pyrolysis of acetylene–ferrocene mixture, showing Fe nanoparticles along with the nanotubes.

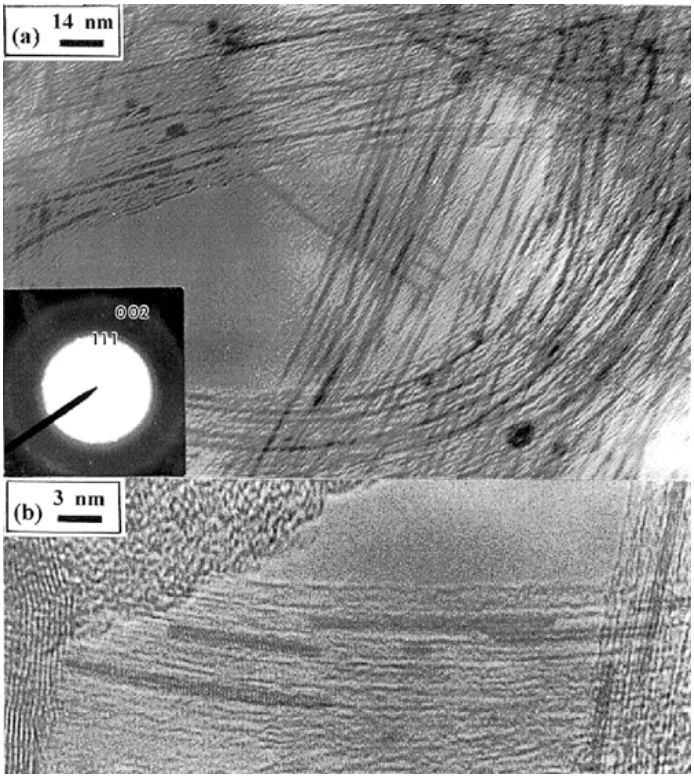

Fig. 12 (a) TEM image of Au nanowires inside SWNTs obtained by the sealed tube reaction. Inset shows a SAED pattern of the nanowires. (b) HREM image showing the single crystalline nature of some of the Au nanowires.

the Fe particles involved in the formation of carbon nanotubes are sufficiently large to render them ferromagnetic. We therefore suggest that the ferromagnetism of the Fe nanoparticles may be responsible for the alignment of the nanotubes produced by pyrolysis of precursors.

METAL NANOWIRES

Metal nanowires encapsulated in carbon nanotubes have been obtained by treating the SWNTs with metal salts at melting temperatures in vacuum-sealed quartz tubes followed by hydrogen reduction [25]. In Fig. 12a, we show a TEM image which reveals the presence of a large number of nanotubes filled extensively with gold. The length of the gold wires so obtained is in the range of 15–70 nm, and the diameters in the range of 1.0–1.4 nm. Selected area electron diffraction (SAED) patterns taken from the region of nanowires (inset of Fig. 12a) shows diffuse rings due to small particles. The diffraction rings correspond to the (111) and (002) reflections of gold. In some of the nanowires, we have found the metal to be single crystalline as shown in the HREM image in Fig. 12b. This image reveals the resolved lattice of gold with a spacing of ~0.23 nm, corresponding to the (111) planes. Polycrystalline Au aggregates could be transformed into single crystalline wires by suitable annealing. UV-vis spectra of dispersions of the gold nanowires in ethanol show transverse plasmon absorption band at ~520 nm and longitudinal bands at 670, 860 and 1150 nm. These bands are an indication of the quantum confinement experienced by the gold nanowires, and also they imply different aspect ratios (3–6) of the wires [26]. Employing similar methods, nanowires of Ag, Pt, and Pd have also been obtained in the capillaries of SWNTs.

REFERENCES

1. J. H. Fendler (ed.). *Nanoparticles and Nanostructured Films*, Wiley-VCH, Weinheim (1998).
2. P. P. Edwards, R. L. Johnston, C. N. R. Rao. In *Metal Clusters in Chemistry*, P. Braunstein, G. Oro, P. R. Raithby (eds.), Wiley-VCH, Weinheim (1999).
3. G. Markovich, C. P. Collier, S. E. Henrichs, F. Remacle, R. D. Levine, J. R. Heath. *Acc. Chem. Res.* **32**, 397 (1999).
4. S. J. Tans, A. R. M. Verschueren, C. Dekker. *Nature* **393**, 49 (1998).
5. C. P. Collier, T. Vossmeyer, J. R. Heath. *Annu. Rev. Phys. Chem.* **49**, 371 (1998).
6. H. N. Aiyer, V. Vijayakrishnan, G. N. Subbanna, C. N. R. Rao. *Surf. Sci.* **313**, 392 (1994).
7. V. Vijayakrishnan, A. Chainani, D. D. Sarma, C. N. R. Rao. *J. Phys. Chem.* **96**, 8679 (1992).
8. R. Busani, M. Follera, O. Chesnovsky. *Phys. Rev. Lett.* **81**, 3836 (1998).
9. K.V. Sarathy, G. Raina, R. T. Yadav, G. U. Kulkarni, C. N. R. Rao. *J. Phys. Chem. B* **101**, 9876 (1997).
10. C. P. Vinod, G. U. Kulkarni, C. N. R. Rao. *Chem. Phys. Lett.* **289**, 329 (1998).
11. M. Rosenblit and J. Jortner. *J. Phys. Chem.* **98**, 9365 (1994).
12. H. N. Vasan and C. N. R. Rao. *J. Mater. Chem.* **5**, 1755 (1995) and references therein.
13. K. R. Hari Kumar, S. Ghosh, C. N. R. Rao. *J. Phys. Chem.* **101**, 536 (1997).
14. M. Brust, M. Walker, D. Bethell, D. J. Schiffrin, R. Whyman. *J. Chem. Soc. Chem. Commun.* **801** (1994).
15. K. V. Sarathy, G. U. Kulkarni, C. N. R. Rao. *J. Chem. Soc. Chem. Commun.* **537** (1997).
16. C. J. Kiely, J. Fink, M. Brust, D. Bethell, D. J. Schiffrin. *Nature* **396**, 444 (1998).
17. L. F. Chi, S. Rakers, J. Drechesler, M. Hartig, H. Fuchs, G. Schmidt. *Thin Solid Films* **329**, 520 (1998).

18. C. P. Collier, R. J. Saykally, J. J. Shiang, S. E. Henrichs, J. R. Heath. *Science* **277**, 1978 (1997).
19. K. V. Sarathy, P. J. Thomas, G. U. Kulkarni, C. N. R. Rao. *J. Phys. Chem. B* **103**, 399 (1999).
20. C. N. R. Rao, A. Govindaraj, R. Sen, B. C. Satishkumar. *Mat. Res. Innovat.* **2**, 128 (1998).
21. M. Terrones, N. Grobert, J. P. Zhang, H. Torrenes, J. Olivares, H. K. Hsu, A. K. Cheetam, H. W. Kroto, D. R. M. Walton. *Chem. Phys. Lett.* **285**, 299 (1998).
22. W. Z. Li, S. S. Xe, L. X. Qian, B. H. Chang, B. S. Zou, W. Y. Zhou, R. A. Zhao, G. Wang. *Science* **274**, 1701 (1996).
23. G. Che, B. B. Laxmi, C. R. Martin, E. R. Fischer, R. S. Ruoff. *Chem. Mater.* **10**, 260 (1998).
24. B. C. Satish Kumar, A. Govindaraj, C. N. R. Rao. *Chem. Phys. Lett.* **307**, 158 (1999).
25. A. Govindaraj, B. C. Satish Kumar, M. Nath, C. N. R. Rao. *Chem. Mat.* **12**, 202 (2000).
26. S. Link, M. B. Mohammed, M. A. El-Sayed. *J. Phys. Chem. B* **103**, 3073 (1999).